Powder Technology 403 (2022) 117381

Contents lists available at ScienceDirect

Powder Technology

journal homepage: www.elsevier.com/locate/powtec

Predictive modelling of powder compaction for binary mixtures using the finite element method

Dingeman L.H. van der Haven [a], Frederik H. Ørtoft [b], Kaisa Naelapää [b], Ioannis S. Fragkopoulos [c,*], James A. Elliott [a,*]

[a] Department of Materials Science & Metallurgy, University of Cambridge, 27 Charles Babbage Road, Cambridge, CB3 0FS, United Kingdom
[b] Oral Formulation Research, Novo Nordisk A/S, Måløv, Denmark
[c] Future Manufacturing & Digital Innovation, Novo Nordisk A/S, Måløv, Denmark

ARTICLE INFO

Article history:
Received 17 January 2022
Received in revised form 4 April 2022
Accepted 6 April 2022
Available online 12 April 2022

Keywords:
Powder compaction
Drucker-Prager Cap model
Predictive modelling
Mixing model
Mechanical properties
Formulation

ABSTRACT

Despite the widespread use of solid-form drug delivery within the pharmaceutical industry, tablets remain challenging to formulate because their properties depend strongly on the powder composition and details of the compaction process. Powder compaction simulations, using the finite element method (FEM) in combination with the density-dependent Drucker-Prager Cap model, can be used to aid the design process of pharmaceutical tablets. Parametrisation is typically carried out manually and requires experimental data for each powder considered. This becomes cumbersome when considering different ratios of component powders. An automated parameterisation workflow was developed and validated using experimental powder mixtures of microcrystalline cellulose and dibasic calcium phosphate dihydrate. FEM simulations reproduced experimental compaction curves with a mean error of 2.5% of the maximum compaction pressure. Moreover, a mixing methodology was developed to estimate parameters of mixtures using only pure-component parameters as input. The experimental compaction curves of mixtures were predicted with a mean error of 4.8%.

1. Introduction

The continued popularity of tablets as a dosage form within the pharmaceutical industry stems from their advantages, such as physical and chemical stability, dosage precision, ease of large-scale production, and patient compliance. However, not all pharmaceutical compounds can easily be made into tablets. Tablet defects such as capping, lamination, or chipping can occur [1–3]. Tablets can also be too porous or too dense, which may affect the gastric residence time and dissolution rate of the tablet and thereby also the release of the active pharmaceutical ingredients (APIs) [4–6]. Defective tablets are costly because of production loss or product recalls [7,8]. It is therefore of major interest to try and prevent these tabletting defects.

The frequency of tabletting defects depends strongly on the formulation and production process [9]. During formulation, the APIs are combined with excipients, such as fillers, disintegrants, or colouring agents. Hereafter, the powder is compressed into a solid tablet, the most common method being direct compression using a tablet press. However, variations in compaction pressure, compaction speed, and punch shape can affect the structural integrity of the tablet and, due to the large number of parameters to be optimised, experimental trial and error is a costly undertaking. This has made computational methods increasingly popular for improving the design and efficiency of the tabletting process.

Although powders are granular materials, typically containing particles with sizes of tens to hundreds of micrometers, continuum models have been successful in predicting potential tablet defects [10,11]. The finite element method (FEM) has frequently been employed to simulate powder compaction at the macroscale and help with the design of the tabletting process. To do so, FEM models need to have an accurate representation of all material properties of the powder. This mechanical behaviour is thus typically defined using an elasto-plastic constitutive model, such as the density-dependent Drucker-Prager cap (dDPC) [12], the metallic foam [13,14], Gurson [15], or modified Cam-Clay models [16]. Experimental data are often used to parametrise the model and obtain FEM predictions that closely mimic experimental results. Such a digital twin approach, in particular using the dDPC model, has had success in predicting the compaction curve, defects, and the tensile strength of tablets [11,12,17–23].

Previous studies have considered either pure excipients or a specific powder formulation (i.e. a mixture). This approach therefore requires

* Corresponding authors.
E-mail addresses: ifra@novonordisk.com (I.S. Fragkopoulos), jae1001@cam.ac.uk (J.A. Elliott).

https://doi.org/10.1016/j.powtec.2022.117381

Nomenclature

d	Cohesion [MPa]
D	Tablet diameter [mm]
$d\lambda$	Magnitude of plastic deformation [-]
E	Young's modulus [GPa]
F_c	Cap yield surface [MPa]
$F_{r,max}$	Maximum radial force [N]
F_s	Shear yield surface [MPa]
F_t	Transition yield surface between F_s and F_c [MPa]
$F_{z,max}$	Maximum axial force [N]
G_c	Plastic flow component associated with F_c [-]
H	Current powder height [mm]
H_0	Initial powder height [mm]
k_b	Constant representing bonding capacity [-]
K	Janssen's constant [-]
$L1$	The $L1$ loss function [-] or [%]
M	Constrained modulus [GPa]
p	Hydrostatic stress or pressure [MPa]
p_a	Hydrostatic stress or pressure [MPa]
p_b	Hydrostatic yield stress or pressure [MPa]
q	Von Mises equivalent stress [MPa]
R	Cap eccentricity [-]
t	Tablet thickness [mm]
w	Weight fraction [-]
y	Volume fraction [-]
y_0	Initial volume fraction [-]
z	Distance with respect to the top punch [mm]
α	Smoothing constant in DPC model [-]
β	Internal friction angle [rad]
ε_v^{el}	True elastic volumetric strain [-]
ε_v^{pl}	True plastic volumetric strain [-]
ε_v^{tot}	Total true volumetric strain [-]
ε_r^{pl}	True plastic radial strain [-]
$\varepsilon_z = \varepsilon_z^{tot}$	Total true axial strain [-]
ε_z^{el}	True elastic axial strain [-]
ρ	Relative density [-]
ρ_0	Relative density of uncompacted powder [-]
ρ_m	Compaction density [g cm^{-3}]
ρ_t	Effective true density [g cm^{-3}]
$\bar{\sigma}$	Limiting fracture stress at $\rho = 1$ [MPa]
$\sigma_1, \sigma_2, \sigma_3$	Principal stresses [MPa]
σ_r	Radial stress [MPa]
σ_r^f	Radial fracture stress [MPa]
σ_T	Axial stress on the top punch [MPa]
σ_z	Axial stress [MPa]
σ_z^f	Axial fracture stress [MPa]
ν	Poisson's ratio [-]

experimental data, and sometimes *ad hoc* fitting procedures, for each and every mixture. This becomes problematic when a wide range of powder mixtures must be considered during the development process, in particular for mixtures in which the ratio of the components is changed. Parametrising the dDPC model for each mixture quickly becomes impractical because of the large quantities of experimental data required. It is thus highly desirable to have a method that only uses data from the single components to predict the behaviour of powder mixtures.

The majority of previous attempts to predict the mechanical properties of tablets made from powder mixtures used statistical, algorithmic, or machine learning models [9,24–28]. Although all of these studies produced predictive models, they require large quantities of experimental data due to the fact that the underlying models were not physically inspired. This makes them less suitable for bottom-up approaches, or when few data are available.

Conversely, the requirements on experimental data can be minimized by incorporating the appropriate physics into a model for powder compaction. Following this rationale, Queiroz et al. proposed a physical model to predict a crossover in the properties of a powder blend based on percolation theory, but this did not distinguish between tablets of different densities and was only defined for binary mixtures [29]. A more complete model, based on volumetric mixing rules, was proposed by Wu et al. and this successfully predicted the tensile strength of mixed-powder tablets [30,31]. Reynolds et al. later showed that a similar model can also be used to predict the compaction curves of mixed-powder tablets [32]. However, their model only makes predictions for the bulk behaviour along the loading path of the compaction curve, giving no details about the stress distribution within the tablet. Nonetheless, this hints that volumetric mixing rules might provide a promising starting point for a physically inspired mixing model.

The aim of this work is to develop a method to i) parametrise the dDPC model for FEM simulations of pure materials in an automated manner and ii) use single-material parametrisations to predict the dDPC model parameters, and thus the compaction behaviour, of powder mixtures. Particular care is taken to avoid *ad hoc* solutions, such that the described procedure can be automated and is valid for all materials considered. Finally, we investigate how the homogeneity of the powder mixture affects the validity of model predictions as well as the axial and radial pressures during compaction.

2. Experimental methods

A range of experimental data are needed for the parametrisation and validation of the FEM compaction model. The current section provides an overview of all the experiments, used materials, and required preprocessing.

2.1. Materials

The materials chosen for this study are micro-crystalline cellulose (MCC) of grade Avicel PH200® and dibasic calcium phosphate dihydrate (DCPD) of grade Emcompress premium®. Material grades were chosen to have similar particle-size distributions (Fig. S1) with a mean diameter ~200 μm.

2.2. Experimental data acquisition

2.2.1. Uniaxial powder compaction

Uniaxial compaction was carried out using a STYL-One Evolution press (Medelpharm, Beynost, France) equipped with a 80 kN load cell, an instrumented cylindrical die, and flat-faced circular punches with a diameter of 11.28 mm. Before each compaction cycle, an external lubrication device (Medelpharm lubrication pack) was used to spray magnesium stearate onto the die and punch surfaces to ensure that the tooling was sufficiently lubricated. A double-ended compaction (DEC) profile was used such that the punches moved in a V-shaped profile with a combined velocity of 0.4 mm s^{-1}, giving quasi-static conditions. The individual punches thus moved at a speed of 0.2 mm s^{-1}. The punches were positioned such that the pressure sensor in the die wall was always halfway the height of the powder compact. The compaction density ρ_m was determined by dividing the mass of the tablet (measured after ejection) by the volume calculated from the current distance between the two punches. The punch positions were corrected for punch deformation. A total of ten tablets were produced per material for each target density.

2.2.2. Automated preprocessing

An automated filtering method was implemented to improve reproducibility and user convenience. This preprocessing step was applied to all compaction data and marks the beginning and ending of each compaction curve by detecting the first and last significant pressure measurements. The initial and final powder heights as well as the punch positions therefore follow immediately. Additionally, a correction was applied to the compaction curves to avoid unphysically large elastic moduli. For details, see supplementary information.

2.2.3. Effective true density

The true density ρ_t, i.e. the density of the completely non-porous material, is determined using the method described by Sun [33]. A tablet is produced by compacting a powder up to a number of high target forces. The true density is then determined using the Kuentz-Leuenberger model (additional detail in supplementary information) [34].

2.2.4. Compression strength tests

The Texture Analyser TA.XT.plusC (Stable Micro Systems, Surrey, United Kingdom) equipped with a 50 kg load cell was used to crush tablets in the radial direction (also known as the Brazilian test), whereas the STYL-One Evolution (Medelpharm, Beynost, France) was used to crush tablets in the axial direction. Assuming a Hertzian contact stress, the fracture stresses can then be estimated from experiment [35,36]. The radial (or diametrical) fracture stress is given by

$$\sigma_r^f = \frac{2F_{r,max}}{\pi D t} \tag{1}$$

and the axial fracture stress by

$$\sigma_z^f = \frac{4F_{z,max}}{\pi D^2}, \tag{2}$$

where $F_{r,max}$ is the maximum radial compression force, $F_{z,max}$ is the maximum axial compression force, D is the tablet diameter, and t is the tablet thickness. Both the radial and axial fracture stresses were determined for three tablets per density for each material or mixture.

The fracture stress depends strongly on the relative density of the tablet. A common choice for describing this dependency is the Rhyshkewitch-Duckworth equation [31,32,37]

$$\sigma^f(\rho) = \bar{\sigma}\exp(-k_b(1-\rho)) \tag{3}$$

where $\bar{\sigma}$ is the fracture stress at $\rho = 1$ and k_b is a constant representing the bonding capacity. The relative density ρ follows from the density of the tablet measured just before the compression strength experiment divided by the true density ρ_t.

2.2.5. Friction between powder and die wall

The friction between the powder and the die wall significantly affects the compaction process and has to be accounted for. In particular, higher wall friction has been associated with increased tablet density and stresses near the die wall and a small increase in overall axial pressure [11,17,19,20]. A typical derivation of the friction coefficient makes use of differential-slice or Janssen-Walker theory [11,38], which in the case of double-ended compaction (DEC) can give the equation (full derivation in supplementary information)

$$\mu = \frac{D}{4zK}\ln\left(\frac{\sigma_T K}{\sigma_r}\right), \tag{4}$$

where σ_T is the top-punch pressure, z is the distance with respect to the top punch, σ_r is the radial pressure at height z, and

$$K = \frac{1+\sin(\beta(\rho))}{1-\sin(\beta(\rho))}. \tag{5}$$

The values for the internal friction angle β are obtained from fracture stress experiments by using Eq. (15). The resulting friction coefficients are between 0.16 and 0.18 for all materials studied here, and appear to be constant with respect to the radial pressure. These values and observations are in line with previous reports [11,17,19,20].

3. Constitutive model and parametrisation

3.1. The density-dependent Drucker-Prager Cap (dDPC) model

The mechanical properties of the powder are described using the density-dependent Drucker-Prager Cap (dDPC) model [10,11]. Experimental data is used to obtain the material-dependent dDPC parameters to fully define the powder behaviour. The stress state of the material is described by the hydrostatic stress,

$$p = \frac{1}{3}(\sigma_1+\sigma_2+\sigma_3) = \frac{1}{3}(\sigma_z+2\sigma_r), \tag{6}$$

where σ_z is the axial stress and σ_r is the radial stress, and the von Mises equivalent stress,

$$q = \sqrt{\frac{(\sigma_1-\sigma_2)^2+(\sigma_2-\sigma_3)^2+(\sigma_3-\sigma_1)^2}{2}} = |\sigma_z-\sigma_r|, \tag{7}$$

which have immediately been simplified for the case of axisymmetric and uniaxial compaction along the z-axis. The dDPC model defines a yield surface that consists of a shear failure segment F_s, a cap F_c, and a transition region F_t (Fig. 1).

Mohr-Coulomb theory is used to define the shear failure segment. The theory states that shear flow occurs starting from the line

$$F_s(p,q) = q - p\tan(\beta) - d = 0 \tag{8}$$

where, d is the cohesion and β the internal angle of friction.

Compressive flow or consolidation can also occur. This happens on the cap of the model, which is given by a curve with constant eccentricity

$$F_c(p,q) = \sqrt{(p-p_a)^2+\left(\frac{Rq}{1+\alpha-\alpha/\cos\beta}\right)^2} - R(d+p_a\tan\ \beta) = 0 \tag{9}$$

where

$$p_a = \frac{p_b - Rd}{1+R\tan\beta} \tag{10}$$

with p_b the hydrostatic yield stress upon compression, R the cap eccentricity, and α a smoothing constant. The function p_b is generally considered to depend on the true volumetric plastic strain ε_v^{pl}, meaning

$$p_b = f(\varepsilon_v^{pl}) \tag{11}$$

and is also called the cap-hardening curve.

To aid numerical implementation, the shear failure segment and the cap are joined together by a smooth transition region

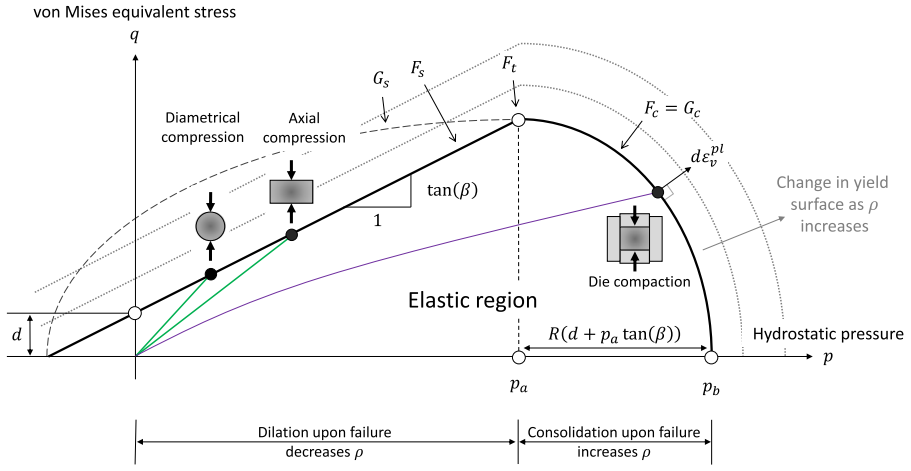

Fig. 1. A yield surface that is defined as a function of the hydrostatic (p) and von Mises equivalent (q) stress as given by the Drucker-Prager Cap (DPC) model. The entire yield surface shifts depending on the density if the density-dependent DPC model is used. As illustrated, experiments can be used to obtain specific points on the yield surface. Figure after Garner et al. [41].

$$F_t(p,q) = \sqrt{(p-p_a)^2 + \left[q - \left(1 - \frac{\alpha}{\cos\beta}\right)(d + p_a \tan\beta)\right]^2} - \alpha(d + p_a \tan\beta) = 0. \tag{12}$$

The material thus undergoes plastic deformation if the stress state of the material is on or outside this yield surface. Otherwise, the material behaves purely elastically according to its Young's modulus E and Poisson's ratio ν.

When using the dDPC model, the location of the yield surface further depends on the relative density ρ of the powder being compacted [11,12,39]. The dDPC parameters d, β, R, and p_b are therefore functions of the relative density. The unitless relative density is defined as

$$\rho = \rho_0 \exp(\varepsilon_v^{pl}) \tag{13}$$

with ρ_0 the unitless relative density of the uncompacted powder in the die, before compression. The value of ρ_0 is taken to be the lowest value of the compaction density ρ_m of all compaction curves of that powder, divided by the true density ρ_t. The lowest values of ρ_m follow from the automated preprocessing mentioned in Section 2.2. We further emphasise that the relative density is thus only dependent on the plastic deformation and that compression is considered to give positive strain. The elastic properties E and ν are also taken to be density-dependent. The rest of this section describes how the dDPC parameters are obtained from experiment.

3.2. Cohesion and internal friction angle

The material cohesion d and internal friction angle β can be obtained from fracture stress experiments [11]. It follows from Eq. (8) that (full derivation in supplementary information)

$$d = \frac{\sigma_z^f \sigma_r^f (\sqrt{13} - 2)}{\sigma_z^f - 2\sigma_r^f} \tag{14}$$

and

$$\beta = \tan^{-1}\left(\frac{3(\sigma_z^f + d)}{\sigma_z^f}\right). \tag{15}$$

Closed-form expressions for $d(\rho)$ and $\beta(\rho)$ may then be obtained by substituting the fracture stresses σ_r^f and σ_z^f that follow from Eq. (3) into Eq. (14) and (15).

3.3. Cap plasticity parameters

Here, we consider the calibration of the plastic parameters R and p_b from uniaxial die compaction, following the approach described by Han et al. [12]. Point A in Fig. 2, the stress peak, is generally considered to be located on the cap of the yield surface. Eq. (9) therefore applies at point A, meaning that $F_c(p_A, q_A) = 0$. Also associated with Eq. (9) is a plastic flow potential component:

$$G_c = \sqrt{(p-p_a)^2 + \left(\frac{Rq}{1 + \alpha - \alpha/\cos\beta}\right)^2}. \tag{16}$$

The associative flow rule in the radial direction is

$$d\varepsilon_r^{pl} = d\lambda \left.\frac{\partial G_c}{\partial \sigma_r}\right|_{p_A, q_A} \tag{17}$$

with $d\varepsilon_r^{pl}$ the change in radial plastic strain, $d\lambda > 0$ the magnitude of the plastic deformation, and the derivative of G_c indicating the direction. Furthermore, the die wall is assumed to be a non-deformable rigid body where the increments in both the elastic and plastic strain are assumed to be zero, giving $d\varepsilon_r^{pl} = 0$. It follows that the change in G_c at this point is also zero:

$$\left.\frac{\partial G_c}{\partial \sigma_r}\right|_{p_A, q_A} = 0. \tag{18}$$

Eq. (18) can then be combined with Eqs. (6, 7), and (16) to give

$$R = \sqrt{\frac{2}{3q_A}(1 + \alpha - \alpha/\cos\beta)^2 (p_A - p_a)}. \tag{19}$$

Hereafter, Eq. (19) is substituted back into Eq. (9) to also obtain

$$p_a = -\frac{3q_A + 4d(1 + \alpha - \alpha/\cos\beta)^2 \tan\beta}{4[(1 + \alpha - \alpha/\cos\beta)\tan\beta]^2} + \frac{\sqrt{9q_A^2 + 24q_A d(1 + \alpha - \alpha/\cos\beta)^2 \tan\beta + 8(3p_A q_A + 2q_A^2)[(1 + \alpha - \alpha/\cos\beta)\tan\beta]^2}}{4[(1 + \alpha - \alpha/\cos\beta)\tan\beta]^2}.$$

Rearranging Eq. (10) finally gives an expression for the hydrostatic yield stress

$$p_b = p_a(1 + R\tan\beta) + Rd. \tag{20}$$

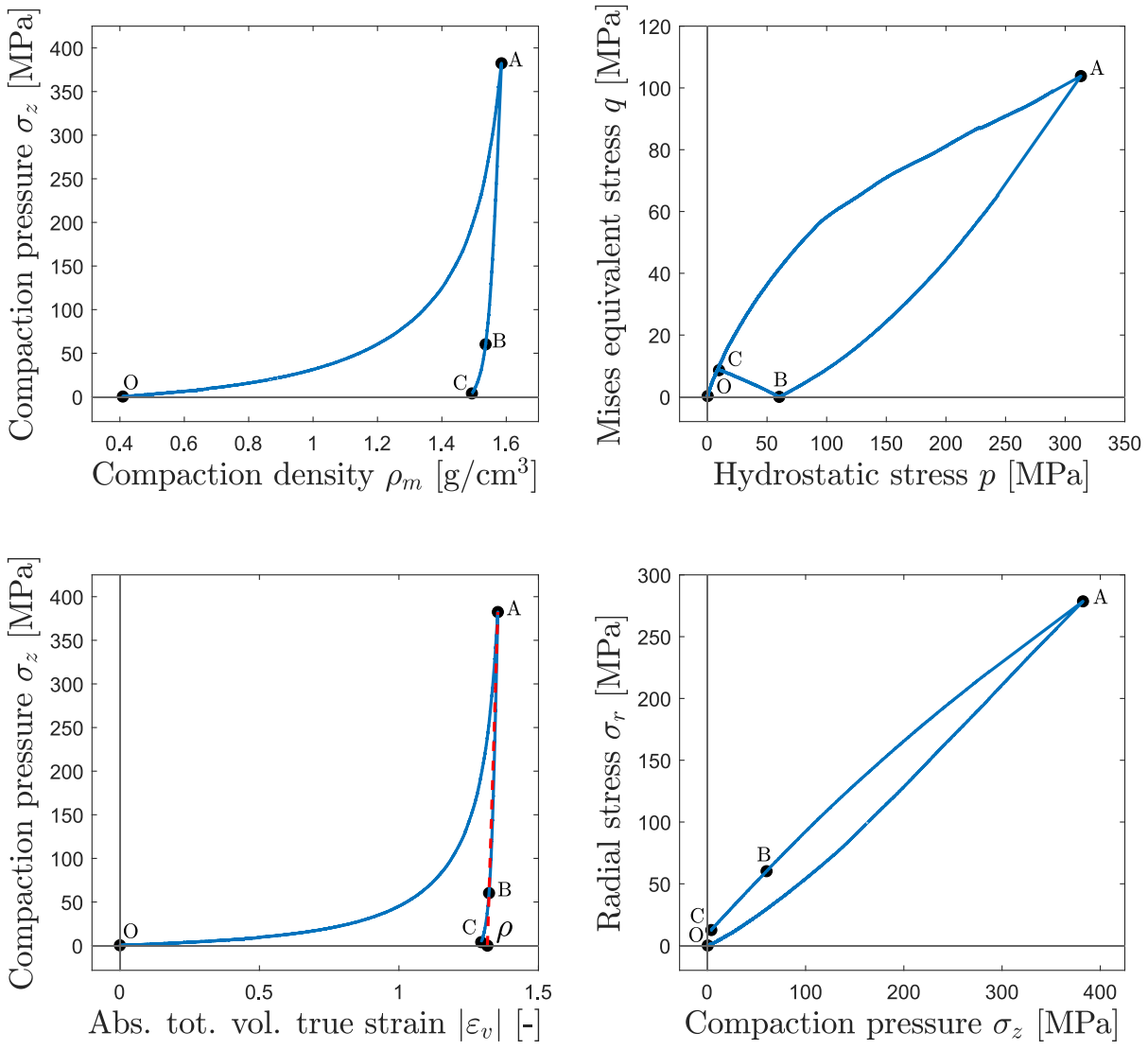

Fig. 2. Different data resulting from a single compaction experiment. Upper left: compaction curve used for validation. Upper right: *p-q* curve used to determine the DPC parameters *R* and p_b. Lower left: stress-stain curve used to determine the Young's modulus and relative density. Lower right: radial to axial stress plot used to determine the Poisson's ratio. Point *O* marks the start of compaction, *A* marks the peak compaction pressure, point *B* marks the point during unloading where $q = 0$, and *C* marks the end of unloading.

The parameters R and p_b can be obtained from uniaxial compaction experiments if d, β, and α are known. The parameters d and β have already been defined using Eq. (14) and (15). The value of α describes the transition between the failure segments and a constant value of 0.03 is used here as in previous studies [40].

3.4. Young's modulus and Poisson's ratio

The elastic parameters are determined using the decompression path of the unaxial die compaction experiments, i.e. segments *AB* in Fig. 2. It is widely presumed that the recovery of the tablet is purely elastic for this part of unloading [10,12,40,20]. In the absence of viscoelastic behaviour, both the hydrostatic and von Mises stress in this part of the curve are monotonically decreasing, making it less likely that internal tablet failure occurs. The slope of the σ_z-ε_z curve (or, equivalently, the σ_z-ε_v curve) can then be used to obtain an expression for E. This results in the expression (full derivation in supplementary information)

$$E = \frac{(1+\nu)(1-2\nu)}{(1-\nu)}\left(\frac{\mathrm{d}\sigma_z}{\mathrm{d}\varepsilon_z}\right). \tag{21}$$

Similarly, the slope of the *AB* segment of the σ_z-σ_r curve can be used to obtain an expression for ν, giving

$$\nu = \frac{\left(\frac{\mathrm{d}\sigma_r}{\mathrm{d}\sigma_z}\right)}{1+\left(\frac{\mathrm{d}\sigma_r}{\mathrm{d}\sigma_z}\right)}. \tag{22}$$

The Poisson's ratio ν is obtained using Eq. (22) after which Eq. (21) is used to estimate the Young's modulus E, giving the values shown in Fig. 3. It is emphasised that elastic parameters are determined using true strains, as is conventional for systems experiencing large deformations.

3.5. Relative density

The relative density is the main variable influencing material properties and should thus be determined carefully. During ejection and the final stages of decompression (segment *BC*), the tablet may undergo shear failure [17]. The von Mises stress increases along segment *BC* and can thus reach the shear failure line in some cases. This can change the relative density of the tablet or make the measurement thereof

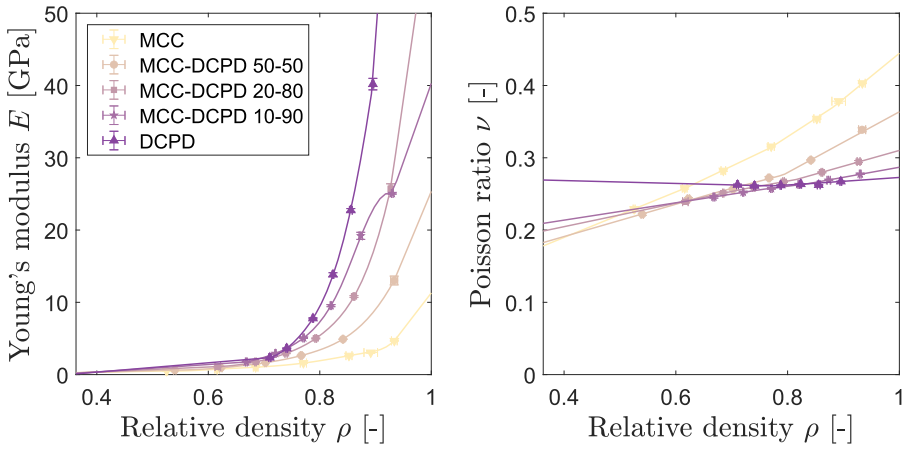

Fig. 3. The Young's modulus and Poisson's ratio as function of the relative density for each powder mixture. Symbols with error bars indicate the mean and standard deviation of the data. The curves are splines with extrapolations as described in the supplementary information (Section S2.4).

infeasible because the tablet fails. Therefore, the true density is estimated by subtracting the true elastic volumetric strain from the volume at the maximum compression point *A*. Only the true plastic volumetric strain remains, which is directly related to the true density, and will likely not yet have been affected by tablet failure during decompression.

Recall that compression is considered to give positive strain and elasticity is assumed to be linear. The elastic strain at point *A* can be expressed as

$$\varepsilon_{\mathrm{v}}^{\mathrm{el}} = \varepsilon_{\mathrm{z}}^{\mathrm{el}} = \int_0^{\sigma_{\mathrm{z,A}}} \frac{1}{M} \mathrm{d}\sigma_{\mathrm{z}} = \frac{\sigma_{\mathrm{z,A}}}{M} \tag{23}$$

with M being the constrained modulus, and the total strain is given by

$$\varepsilon_{\mathrm{v}}^{\mathrm{tot}} = \varepsilon_{\mathrm{z}}^{\mathrm{tot}} = \ln\left(\frac{H}{H_0}\right) = \ln\left(\frac{\rho_{\mathrm{m,A}}}{\rho_0 \rho_{\mathrm{t}}}\right), \tag{24}$$

where ρ_{m} is the compaction density in g cm^{-3}. Eq. (23) and (24) can then be combined with Eq. (13) to give

$$\rho = \rho_0 \exp\left(\varepsilon_{\mathrm{v}}^{\mathrm{pl}}\right) = \rho_0 \exp\left(\varepsilon_{\mathrm{v}}^{\mathrm{tot}} - \varepsilon_{\mathrm{v}}^{\mathrm{el}}\right) = \frac{\rho_{\mathrm{m,A}}}{\rho_{\mathrm{t}}} \exp\left(-\frac{\sigma_{\mathrm{z,A}}}{M}\right), \tag{25}$$

where M is calculated from E and ν using the definition of the constrained modulus. The red dashed line in Fig. 2 illustrates how the relative density ρ is determined starting from point *A*. By compacting a powder using various pressures, we automatically obtain dDPC and elastic parameters for various relative densities ρ.

Once all parameters have been determined, they can be supplied to the simulation software (see Section 5) in tabulated form. However, parameters have only been determined for a limited number of tablet densities. Furthermore, simulations may locally reach density values outside the range of experimentally measured densities. For these reasons, parameters were interpolated and extrapolated using an approach similar to that of Garner et al. [41]. Details hereof as well as a visual overview of the parametrisation workflow can be found in the supplementary information.

3.6. Quantifying the difference between two compaction curves

To be able to compare two different compaction curves quantitatively, the L1 loss function is introduced

$$L1 = \left(\int_{\rho_{\mathrm{start}}^{\mathrm{ref}}}^{\rho_{\mathrm{end}}^{\mathrm{ref}}} \left|\sigma_{\mathrm{z}} - \sigma_{\mathrm{z}}^{\mathrm{ref}}\right| |\mathrm{d}\rho_{\mathrm{m}}|\right) \times \left(\max\left(\sigma_{\mathrm{z}}^{\mathrm{ref}}\right) \times \int_{\rho_{\mathrm{start}}^{\mathrm{ref}}}^{\rho_{\mathrm{end}}^{\mathrm{ref}}} |\mathrm{d}\rho_{\mathrm{m}}|\right)^{-1} \tag{26}$$

where one of the two curves, denoted with superscript *ref*, is considered to be the reference curve. The L1 loss function gives the deviation of a compaction curve with respect to a reference curve as an average per line segment, normalised by the peak compaction pressure. The modulus signs around $\mathrm{d}\rho_{\mathrm{m}}$ are to assure that the errors of compression and decompression do not cancel out. Eq. (26) gives a fraction but the L1 loss function is also frequently reported as a percentage.

4. Mixing methodology

In line with the main objective of this study, we formulate a set of mixing rules to estimate a model parameter $\theta(\rho)$ for an arbitrary powder mixture at a given relative density ρ. This also means that the relative density ρ of the mixture has to be estimated.

The model by Reynolds et al. inherently assumes that the stress is homogeneous throughout the tablet for all materials (i.e. the isostress assumption for composites) [32]. We therefore start with the assumption that the stress or compaction pressure is indeed equally distributed between all components. All model properties therefore need to be expressed as a function of the compaction pressure σ before any mixing rule can be applied. The compaction density of each single-component powder i is expressed as a function of the compaction pressure, i.e. $\rho_{\mathrm{m},i}(\sigma)$, by fitting a spline. The function $\rho_{\mathrm{m},i}(\sigma)$ is therefore nothing more than the loading path of the compaction curve. The spline $\rho_{\mathrm{m},i}(\sigma)$ is then substituted into a fit that gives the out-of-die relative density as a function of the in-die compaction density (example in supplementary information) to get $\rho_i(\sigma)$, i.e. the relative density as a function of the stress. The function $\rho_i(\sigma)$ is then substituted into the previously-determined parameter functions to define all material parameters of each component i as a function of stress.

Next, we presume that the properties of the mixture also depend on the relative volume that the components occupy. Since the volume fractions of each component are not constant during compression, these also have to be determined as a function of stress. The total stain per component is

$$\varepsilon_{\mathrm{v},i}(\sigma) = \varepsilon_{\mathrm{v}}^{\mathrm{el}} + \varepsilon_{\mathrm{v}}^{\mathrm{pl}} = \int_0^{\sigma} \frac{1}{M_i(\rho_i(\sigma))} d\sigma + \ln\left(\frac{\rho_i(\sigma)}{\rho_{0,i}}\right) \tag{27}$$

where Eq. (23) and the inverted Eq. (13) have been substituted. The constrained modulus M_i follows from the known functions for the

elastic parameters. These strains define the change in volume for each component and can thus be used to determine the volume fractions y_i of component i as a function of compaction pressure:

$$y_i(\sigma) = y_{0,i} \exp\left(-\varepsilon_{v,i}(\sigma)\right) \left(\sum_j y_{0,j} \exp\left(-\varepsilon_{v,j}(\sigma)\right) \right)^{-1}. \quad (28)$$

The initial volume fractions $y_{0,i}$ can be estimated using

$$y_{0,i} = \left(\frac{w_i}{\rho_{0,i}\rho_{t,i}} \right) \left(\sum_j \left(\frac{w_j}{\rho_{0,j}\rho_{t,j}} \right) \right)^{-1} \quad (29)$$

where $\rho_{t,i}$ and w_i are the true density and weight fraction of the respective constituent material [32].

The relative density of the mixture then follows as

$$\rho(\sigma) = \frac{1}{\rho_{t,mix}} \sum_i y_i(\sigma)\rho_i(\sigma)\rho_{t,i} \quad (30)$$

where the true density ρ_t of a mixture can be estimated using the volumetric mixing rule [31,33]

$$\rho_{t,mix} = \left(\sum_i \frac{w_i}{\rho_{t,i}} \right)^{-1}. \quad (31)$$

Finally, the value of any property θ for the mixture is given by

$$\theta(\rho) = f(\theta_1(\rho_1), \ldots, \theta_n(\rho_n), y_1(\rho_1), \ldots, y_n(\rho_n)) \quad (32)$$

with $f(\ldots)$ being the appropriate mixing rule and all the relative densities following from $\rho_i(\sigma)$ and Eq. (30) at the same stress σ. In accordance with the isostress model, the mixing rules for the Young's modulus and the Poisson's ratio are chosen to be the harmonic and arithmetic mean, respectively. For all other parameters the arithmetic mean is used. The arithmetic mean is $f(\theta_1(\rho_1), \ldots, \theta_n(\rho_n)) = \sum_i y_i(\rho_i)\theta_i(\rho_i)$, and the harmonic mean is $f(\theta_1(\rho_1), \ldots, \theta_n(\rho_n)) = \left(\sum_i \frac{y_i(\rho_i)}{\theta_i(\rho_i)} \right)^{-1}$. A visual overview of the parameter mixing workflow can be found in the supplementary information.

For particle interaction models, the weighting in mixing rules is typically made using the surface-area fractions instead of the volume fractions, but the results are the same if the particle sizes are equal. If the particle sizes differ strongly, the extent to which the mixing rules have to be adjusted will depend on the parameter under consideration and how well the isostress assumption holds. For example, parameters such as the cohesion d will depend strongly on the contact area between particles and would need a mixing rule using surface area fractions instead. On the contrary, mixing rules for the elastic parameters E and ν would not change provided that the isostress assumption remains valid because the assumption imposes volume weighting of each component.

The limits of the mixing methodology clearly depend on how well the assumptions hold. Therefore, to test the assumptions of the mixing methodology, a number of inhomogeneous or segregated mixture tablets were also simulated. The different components interacted by means of volume exclusion. The initial densities of each component follow from the mass conservation of the total system. The ejection phase was not simulated for the inhomogeneous tablets as its layers would separate because cohesion was neglected in the present study.

5. Numerical modelling

The commercial software Abaqus 2019 by Simulia was used for all FEM simulations [42]. A FORTRAN script with the Abaqus-defined user-subroutine USDFIELD was used to define a field of relative densities that allowed the density dependence of the dDPC model (example script in supplementary information). A schematic drawing of the model geometry can be seen in Fig. 4. The in-die and punch diameters were set to 11.28 mm. The compaction profile was simulated as a V-shaped DEC profile. The initial and final heights of the powder were set to the averages of all compaction experiments with the same target density. The total mass m of the powder is then given by $m = V_0\rho_0\rho_t$, where V_0 is the initial volume, ρ_0 is the initial relative density as in Eq. (13), and ρ_t is the true density. The compaction density ρ_m follows from the total mass m divided by the volume between the punches, which is calculated using the distance between the punch nodes that touch the powder and lie on the symmetry axis depicted in Fig. 4. Since the thickness of the tablets produced was approximately equal, the final density of a tablet is mainly determined by how much powder mass is filled into the die, i.e. the initial height of the powder.

All parts of the model were represented as axisymmetric deformable bodies because, although only minor, the tooling also shows

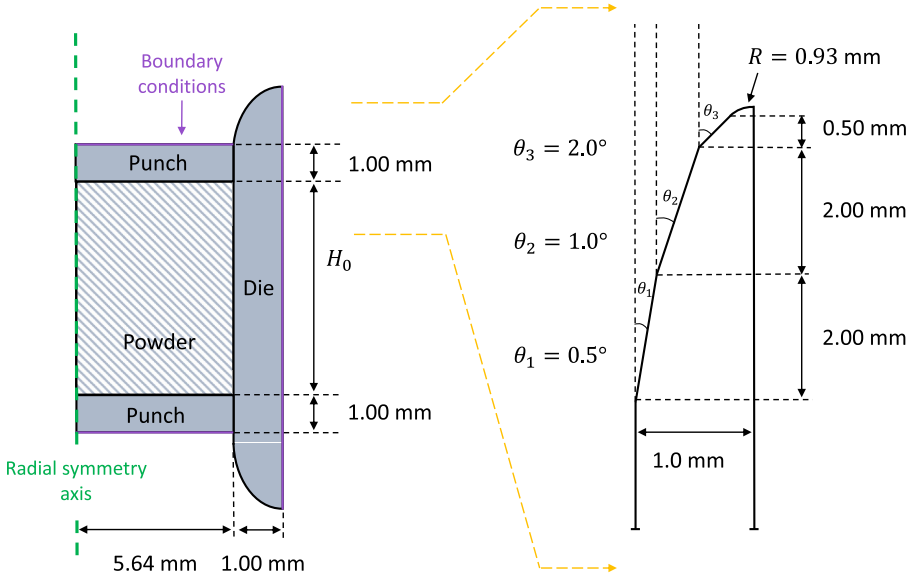

Fig. 4. Schematic drawing of the tooling geometry at the beginning of the simulation. The gradient of the die wall is continuous at the point where the tapering starts to curve outwards. Surfaces constrained by the boundary conditions have been coloured purple. Dimensions are not to scale.

deformations. A uniform, regular mesh with square elements was used for the powder (4312 to 7840 elements, CAX4) and the punches (376 elements, CAX4R). The die was described by an irregular mesh (1294 elements, CAX4R and CAX3) made out of rectangular as well as triangular elements. The area of the elements (in the 2D slice of the axi-symmetric representation) was about 1.0×10^{-2} mm^2 for all parts of the model. The punches and die wall were made to be 1.0 mm thick and given the properties of tooling steel ("Elastic": $E = 210$ GPa, $\nu = 0.3$, "Plastic": yield stress going from 1400 to 1800 MPa for a plastic strain going from 0 to 0.4, and "Density": 7900 kg m^{-3}) [43]. Boundary conditions were applied to the outer surfaces of the punches and die by fixing the positions and rotations. This means that the position of the outer surface of the die was fixed and vertical displacements were applied on the uppermost part of the top punch and lowermost part of the bottom punch. No rotations were allowed for the aforementioned surfaces. The displacement of the punches was determined using the initial and final heights of the experimental tablets.

In the case of materials with very low cohesions and friction angles, the tablet can bend strongly upon ejection due to the sudden release of residual radial pressure. Tapering was therefore added to give a smoother release of the residual radial pressure and avoid excessive bending of the tablet. For some high-density tablets, the initial height of the powder can cause the powder bed to start above the starting point of the tapering. However, compaction simulations with and without tapering show that this has no visible effect on the resulting compaction pressures and density profiles.

Upon testing the used combination of the parametrisation and model geometries, convergence was found to be excellent. The L1 loss function of the compaction curves only changed by 0.027% when going from 476 to 7840 elements for the powder. This is equivalent to going from element areas of 1.7×10^{-1} mm^2 to 1.0×10^{-2} mm^2. We note that it is also possible to construct a 3D model with the current parametrisation but that there is no added benefit in doing so if the system is axisymmetric [20,23].

6. Results and discussion

6.1. Compaction simulations using the automated dDPC parametrisation

The success of a FEM compaction model depends on obtaining an accurate parametrisation of the powder. This is often one of the most challenging aspects in computational studies and typically requires new efforts and solutions for each material. We thus attempted to automate and standardise the parametrisation with a new procedure. This procedure was used to obtain model parameters using experimental data of MCC, DPCD, and all mixtures thereof. The resulting parameters were subsequently used to perform FEM simulations of the compaction process and replicate the compaction curves, one simulation for each combination of material and target density.

Plotting both the simulated and experimental curves in Fig. 5 shows that simulations are able to reproduce the experimental compaction curves of each powder considered. To avoid clutter, Fig. 5 was plotted using only one of the experimental compaction curves. A total of ten curves (each corresponding to an independent tablet) were produced per unique combination of powder mixture and target density, giving ten duplicates. However, due to experimental variability, the accuracy of a simulation naturally depends on which of these duplicates is chosen as reference. We therefore decided to quantify the experimental variability as well as the accuracy of each simulation with respect to all duplicates. The experimental variability was quantified by computing the L1 loss function (Eq. (26)) for all possible duplicate pairs, giving an average L1 of 1.2% of the peak compaction pressure (Fig. S11). The L1 was also used to quantify the simulation error. For each simulation, Fig. 6 shows the resulting mean and standard deviation of the L1 with respect to all experimental duplicates. The simulations again show excellent correspondence with experiment, giving mean L1 values between 0.8 and 5.7% with an overall mean of 2.5%, only marginally larger than the average experimental variability of 1.2%.

A closer inspection of the compaction curves shows that the compaction pressure decreases nonlinearly upon unloading, whereas the simulations predict a linear decrease of the pressure. The difference in unloading behaviour contributes strongly to the mean L1, which decreases by as much as 74% if only the loading path is considered. This also explains the trend observed in Fig. 6, where tablets with a higher density, and thus a longer loading curve, result in a lower average L1. The parametrisation would thus most notably benefit from an improved description of the unloading behaviour. The FEM simulations predict a linear decrease of the compaction pressure because the Young's modulus is independent of the time and stress. The nonlinear unloading behaviour of tablets has been explained through viscoelastic behaviour [44], a stress-dependent Young's modulus [12], and the occurrence of dilation due to shear failure [20,45]. However, no visible failure occurred for our tablets other than those of 90% and 100% DCPD, as will be discussed further on. Viscoelastic behaviour is possible but less likely given the quasi-static conditions resulting from the low decompression

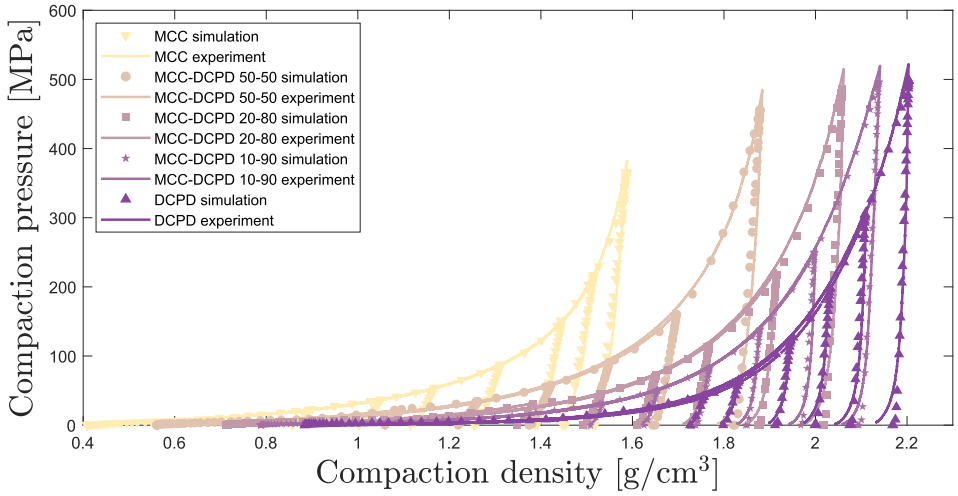

Fig. 5. FEM simulations were able to reproduce the compaction behaviour as shown in experiment for all materials and target densities. For each material, model parameters were obtained from experiment using the automated dDPC parametrisation. Experimental curves are shown for one out of ten tablets, i.e. duplicates, per unique combination of material and target density.

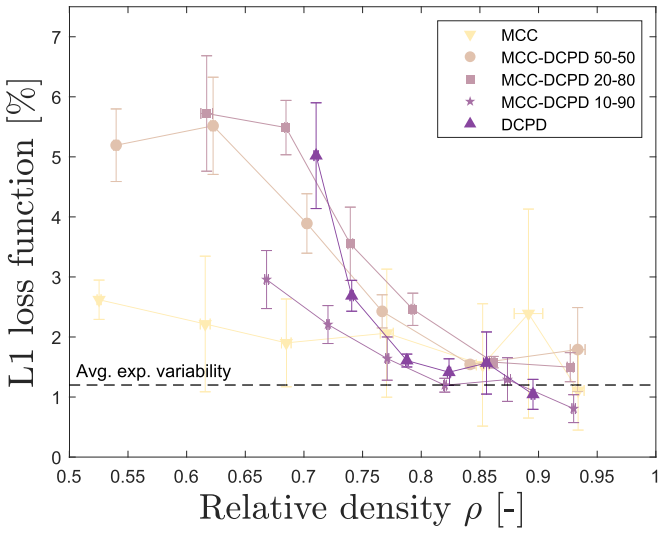

Fig. 6. Computing the L1 loss function (Eq. (26)) shows that the FEM simulations in Fig. 5 are able to reproduce the experimental compaction curves with errors of a few percent. The L1 loss function of each simulated curve was computed, using the experimental curve as reference, and given as a percentage of the peak compaction pressure of the reference curve. This was repeated for all ten experimental curves, i.e. duplicates, produced per unique combination of material and target density. The resulting mean and standard deviation of the L1 loss function are shown here.

speed of 0.4 mm s^{-1}. This suggests that a stress-dependent Young's modulus is the most likely cause of nonlinear unloading behaviour.

A stress-hardening Young's modulus could also help to improve predictions of the residual radial pressure that are currently being overestimated by the simulations. Implementing a stress-dependent Young's modulus would thus be the most impactful improvement to the current parametrisation method. Various implementations have already been proposed by other authors [12,18,44,46,47]. However, to avoid interference with other parts of the parametrisation and minimize the added experimental effort, we recommend future studies to use the modified compaction experiments as suggested by Mazel et al. to parametrise the Young's modulus as a function of the relative density and stress [48]. Nevertheless, without the suggested improvements the agreement between compaction curves validates the proposed parametrisation procedure, giving an accurate representation of all powders considered without the need for user input or other *ad hoc* solutions. Although the parametrisation made use of all duplicates to determine the model parameters, using a minimal dataset only changes the resulting L1 loss functions by ±1%, further showing that the parametrisation is also robust (Fig. S12 to S14). The proposed method thus provides a key step in the development of an automated and standardised parametrisation methodology for the dDPC model, making FEM predictions more reliable and time efficient.

During our experiments, some of the tablets with a high DCPD content showed a chipping defect at the bottom (Fig. 7). These and other potential tabletting defects can be identified based on the stress patterns within the tablet. For example, a band of high shear stress arching from the middle to the tip of the tablet has been related to capping [17,40]. In line with previous studies, we therefore tried to see if this defect could be explained based on the stress profiles within the tablet. Simulations predicted high shear stresses near the bottom edge of the tablet during ejection (Fig. 8). The shear stress at this location furthermore rapidly changes sign. The locus of this feature has been shown to coincide with internal cracks in the tablet, thereby suggesting a chipping mechanism similar to the capping mechanism proposed by Wu et al. [17,40]. We therefore postulate that the chipping at the bottom of the tablet occurs during ejection and is caused by a concentration of shear stress with alternating sign. These results illustrate how FEM simulations can be used to identify potential tabletting defects that occur during the compaction cycle.

6.2. Validation of the mixing methodology

We formulated a mixing methodology to derive FEM model parameters for powder mixtures. The aim of this methodology is to bypass the need for experimental data of the mixture itself, using only the model parameters of the constituent powders. We proceed to validate these mixing rules by using the model parameters of pure MCC and pure DCPD to predict the correct model parameters of the three different MCC-DCPD mixtures.

Prediction of the model parameters for the mixtures started by determining the true density of the mixtures, because the model parameters depend on the relative density, and thereby on the true density, of the mixture. True densities were estimated using Eq. (31), giving deviations of +0.4%, −1.5%, and −2.7% with respect to the experimental true densities for the MCC-DCPD mixtures of composition 50–50, 20-80, and 10–90, respectively. Eq. (31) is therefore considered to be accurate, as was also demonstrated by Wu et al. [31]. Next, we applied the proposed mixing methodology (Eq. (27) to (32)) with the pure MCC

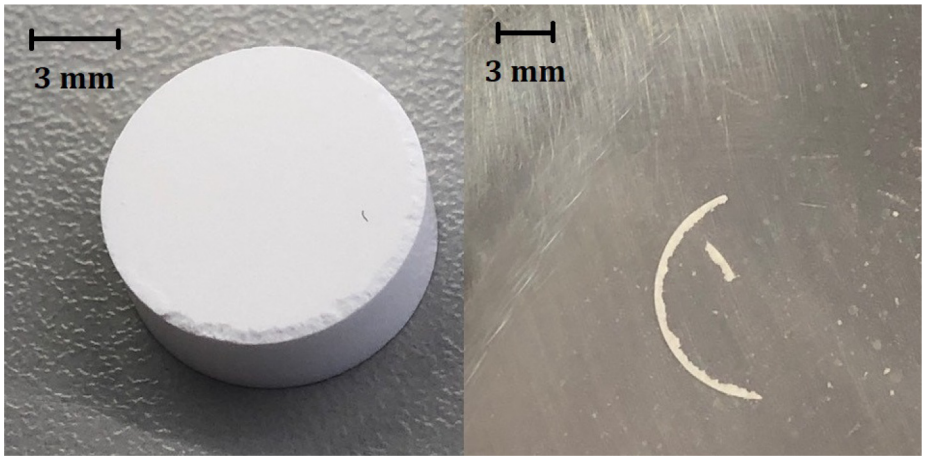

Fig. 7. Chipping occurs at the bottom edge of the tablet for the two most dense 100% DCPD tablets and the most dense tablet with 10% MCC and 90% DCPD. The left image shows the damage on the tablet and the right image shows the trail of compacted powder that was left behind by the chipped tablet. Pictures were taken on a lab bench, after the tablet had been removed from the die.

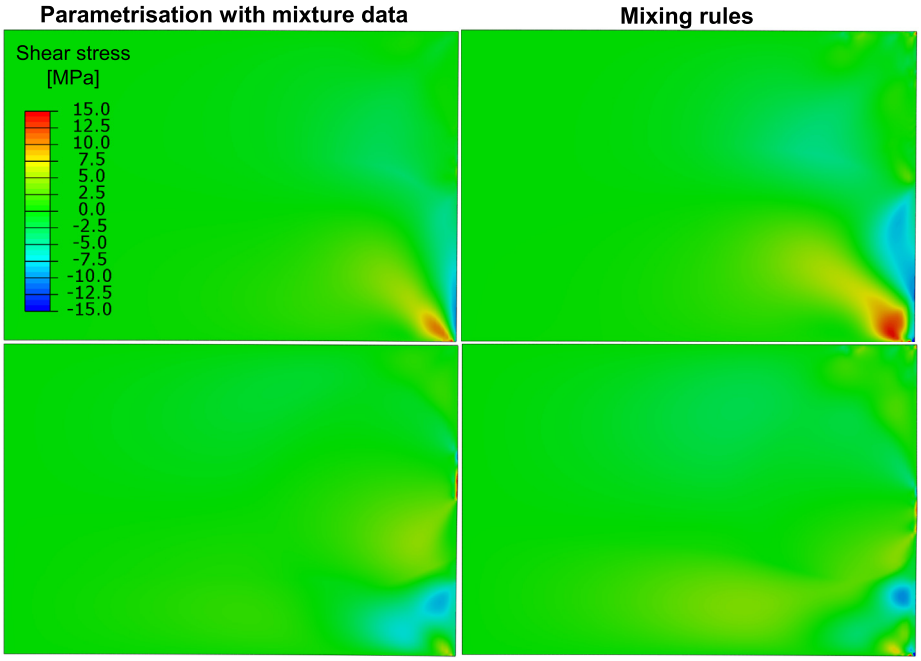

Fig. 8. During ejection, the stress profiles from the FEM simulations predict a concentration of shear stress σ_{12} at the bottom edge of the tablet, the same location as the chipping defect shown in Fig. 7. The stress profiles are those of the highest-density tablet with 10% MCC and 90% DCPD just as the middle of the tablet starts to lose contact with the die (top row) and briefly thereafter (bottom row). FEM simulations were parametrised using either the experimental data of the mixture (left column) or the mixing rules (right column). The stress profiles shown have been generated with a larger number of mesh elements (23 072 to 27 776) for visualisation purposes only.

and pure DCPD parameters as input to produce a complete set of model parameters for each of the three MCC-DCPD mixtures.

FEM simulations performed with the generated parameters, using the mixing methodology, were able to accurately predict the compaction behaviour of each powder mixture (Fig. 9). The L1 varies from 2.0 to 13.8% with a mean of 4.8% (Fig. 10), which is slightly more (by 2.3%) than the simulations parametrised with the experimental data of the powder mixtures. Comparing to previous studies, the compaction pressure can also be predicted using the model of Reynolds et al. [32], resulting in L1 values ranging from 0.8 to 10.0% with a mean of 3.1% (Fig. S15 and S16). The Reynolds et al. model is marginally more accurate (by 1.7%) but is unable to make predictions for the stress profiles nor the axial pressure during decompression. The proposed mixing methodology thus provides a greater predictive power whilst maintaining similar accuracy, opening up the possibility to identify potential tabletting defects of experimentally untested materials.

Aside from similar compaction curves, it is essential that the different parametrisation methods predict similar stress profiles, because the potential tabletting defects identified depend on these. A side-by-side comparison of the von Mises stress profiles generated using either

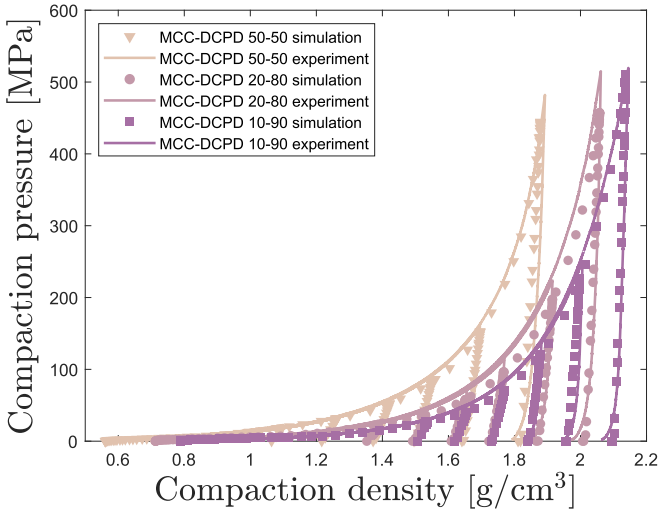

Fig. 9. Using the mixing methodology, FEM simulations are able to predict the compaction behaviour as shown in experiment for all powder mixtures and target densities. For each powder mixture, model parameters were obtained using experimental data of pure MCC and pure DCPD in combination with the mixing methodology. Experimental curves are shown for one out of ten tablets, i.e. duplicates, per unique combination of material and target density.

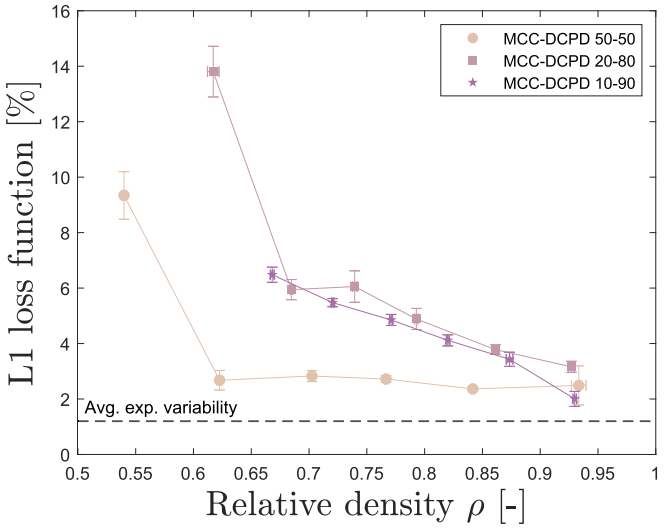

Fig. 10. Computing the L1 loss function (Eq. (26)) shows that the FEM simulations in Fig. 9 were able to predict the experimental compaction curves with errors of a few percent of the peak compaction pressure. The resulting mean and standard deviation of the L1 loss function are shown here, computed for each simulation with respect to all experimental duplicates.

parameters from the mixing rules or the experimental data showed that the profiles are qualitatively similar (Fig. 8, S14, and S15). The magnitude of the stress differs between the parametrisation methods, in most cases less than 10%, but both methods produce similar trends as a function of tablet composition (Fig. S17 and S18). Furthermore, the mixing rules also predicted a concentration of high shear stress, with alternating sign, near the bottom edge of the tablet (Fig. 8). The mixing methodology thus provides a novel tool for the prediction of the compaction pressure and stress profiles of untested powder mixtures.

The current implementation of the mixing methodology was limited to binary mixtures. However, validation of the mixing methodology for ternary and quaternary mixtures is of great interest as this allows for predictions of more realistic powder formulations. A validation for ternary mixtures is an ongoing research focus of the authors. Other topics of interest include a more extensive validation against particles of more different sizes, shapes, and materials. A database of single-component parameters could be used to predict the compaction behaviour of powder mixtures in a mix-and-match type of fashion. Nonetheless, some single-component powders may be difficult to handle, making the extraction of their dDPC model parameters troublesome due to the lack of experimental data. A possible solution would be to invert the proposed mixture rules such that the model parameters of a given component may be extracted from experimental data of a mixture containing this component, given that the parameters of the other components are known.

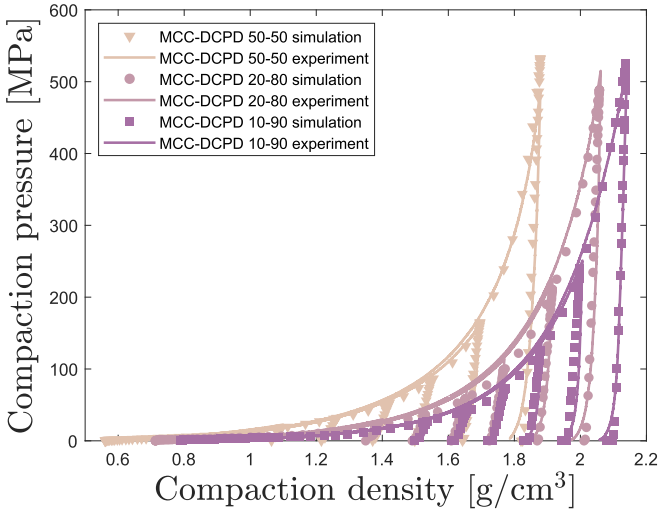

Fig. 11. Using the inhomogeneous tablets with two horizontal layers, FEM simulations are able to predict the compaction behaviour as shown in experiment for all homogeneous powder mixtures and target densities. For each tablet, the model parameters of pure MCC and pure DCPD resulting from experimental data were used after which the volume and density of the initial layers was adjusted as described in the supplementary information. Experimental curves are shown for one out of ten tablets, i.e. duplicates, for each unique combination of material and target density.

6.3. The effect of mixture homogeneity within tablets

A crucial assumption of the mixing methodology proposed in this study is the isostress condition, i.e. that the stress experienced by each component material is the same. If this assumption holds, then an inhomogeneous or layered tablet should predict compaction pressures similar to those predicted by the mixing methodology, given that the components have been arranged to create similar stresses in each component. Furthermore, the use of multi-layered tablets has become increasingly popular as a way to tune drug-release properties or keep incompatible APIs separate [49,50]. Investigating the compaction behaviour of various inhomogeneous tablets is therefore a valuable research topic in itself but also helps us to understand why the proposed mixing methodology works and what its limits are.

We proceeded to test how inhomogeneous tablets with near-isostress conditions compare to the homogeneous binary mixtures. Arranging the tablet in two horizontal layers creates these near-isostress conditions because the stresses in the top and bottom half of the tablet are roughly similar. This similarity is a result of the double-ended compaction (DEC) profile that symmetrical for equal punch speeds. For each binary mixture, we thus simulated a tablet with two horizontal layers that gave the same overall composition. Fig. 11 shows that the compaction pressures of horizontally layered tablets closely follow that of the homogeneous mixtures. The L1 loss function of the horizontally layered tablets with respect to the homogeneous experimental mixtures varied from 1.4 to 14.0% with a mean of 4.5% (Fig. 12), a performance similar to the mixing methodology. For binary mixtures, a corresponding compaction behaviour between horizontally layered and homogeneous tablets has also been reported by Wu and Seville [51]. These agreements between the horizontally layered tablets, predicted homogeneous tablets, and homogeneous experimental tablets imply that the isostress condition is indeed a reasonable assumption.

The suitability of the isostress condition also implies that increasing the number of horizontal layers should not change the compaction behaviour. Furthermore, flipping the tablet vertically should not change the compaction behaviour. A non-exhaustive set of simulations was done, featuring tablets with multiple layers, to test these two assertions. A single mesh was used but nodes were given different material properties based on the assigned layers. These simulations suggest that these assertions are indeed correct, as the variation in the compaction pressures was minimal between the different multi-layered tablets. Notably, the assertions also appear to hold well for an odd number of layers. This is somewhat surprising because an odd number of layers shifts the mass distribution of one of the two components more towards the perimeter of the tablet, breaking the symmetry about the middle of the tablet. However, using non-flat punches will result in larger stress differences, as the material near the punches will typically undergo much more deformation. In such cases a bilayer tablet may no longer resemble the binary mixtures and the use of a mixing methodology becomes a necessity. Nevertheless, the tentative validity of these assertions further supports the appropriateness of the isostress condition to describe the compaction behaviour of multi-component mixtures.

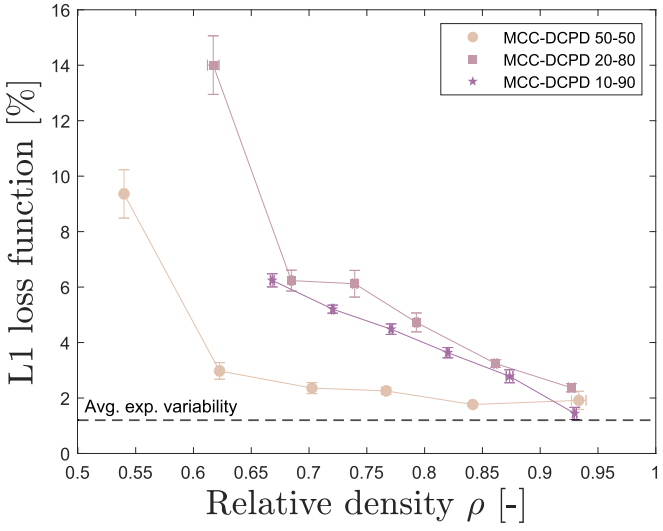

Fig. 12. Computing the L1 loss function (Eq. (26)) shows that the FEM simulations in Fig. 11 were able to predict the experimental compaction curves with errors of a few percent of the peak compaction pressure. The resulting mean and standard deviation of the L1 loss function are shown here, computed for each simulation with respect to all experimental duplicates.

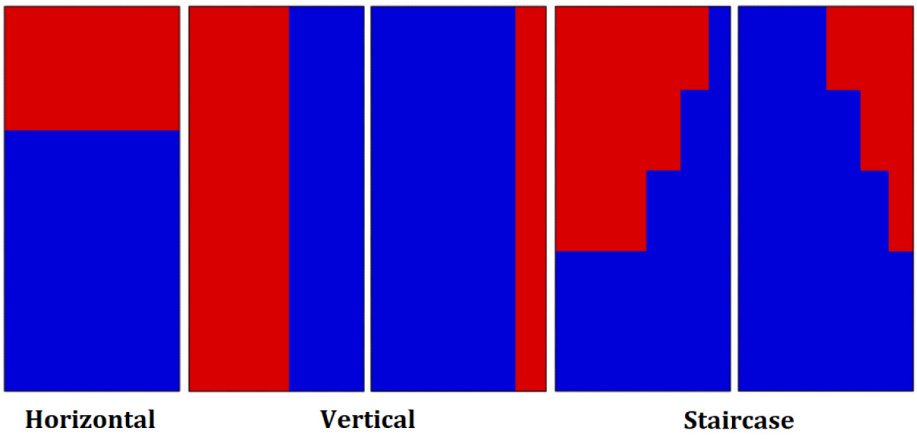

Fig. 13. Cross-sections of the initial spatial arrangements or configurations for the inhomogeneous-mixture tablets that have been considered in this study. Only half of the cross-section is shown with the left boundary corresponding to the central axis and the right boundary to the perimeter of the tablet. All tablets are 50% MCC and 50% DCPD by weight. Blue indicates the MCC powder whereas red indicates the DCPD powder. Note that the areas of the layers within the cross-section differ because of the radial symmetry and the difference in density.

Taking an inhomogeneous tablet with equal weights of MCC and DCPD, we also investigated a number of other spatial configurations (Fig. 13) to see if the correspondence between the inhomogeneous and homogeneous tablets is unique to horizontally layered tablets. The configurations were chosen to resemble different composite models, i.e. the isostress model (horizontal), the isostrain model (vertical), and a mixture of the two (staircase). Simulations featuring these various configurations show that the configuration mainly affects the compaction pressure at intermediate densities (Fig. 14). Vertical layers increase the compaction pressure, because DCPD is carrying most of the load by resisting deformation more than MCC, with the pressure increase being stronger if DCPD is placed at the die wall. This can be explained by vertical layers creating more isostrain-like conditions. The staircase configurations appear to follow the behaviour of the homogeneous mixture slightly more closely (with an L1 that is ~2% lower) than the horizontal configuration. However, the staircase configuration creates conditions that lie somewhere in between isostress and isostrain, making it hard to derive a straightforward mixing rule. Nonetheless, this shows that predictions made by the mixing methodology are insensitive to small changes in the homogeneity of the powder mixture.

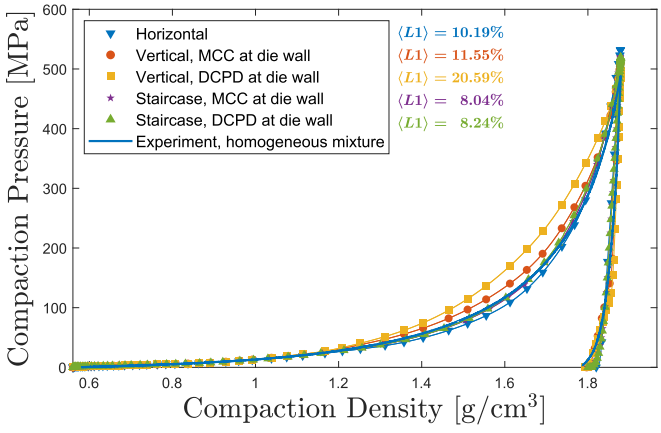

Fig. 14. FEM simulations show that bilayer tablets with a horizontal or staircase configuration result in similar pressures as the homogeneous binary mixture. Compaction curves are shown for various spatial configurations (shown in Fig. 13) of two segregated layers of MCC and DCPD. All tablets were 50% MCC and 50% DCPD by weight, compacted to the highest target density. For each arrangement, the mean L1 loss function is given with respect to the binary mixture with the same powder contents. Compaction density is given for the entire tablet.

A closer look revealed that the spatial configuration of the layers in the tablet had a pronounced effect on the residual radial stress. It appears that placing the softer material at the perimeter of the tablet lowers the residual radial stress σ_r^{res} as well as the ratio of residual radial to maximum axial stress $\sigma_r^{res}/\sigma_z^{max}$ (Table 1). For example, for a tablet with vertical layers, the aforementioned stress (and stress ratio) is lower when MCC is near the perimeter than *vice versa*. The softer material appears to cushion the pressure from the harder material on the die wall. For the configurations considered, this trend appears consistent within different configuration types (i.e. vertical or staircase) as well as across configuration types. The current study is however limited by the lack of a detailed description of the interaction between the different powders in the tablet. This prevented simulations of the ejection stage, which can be just as important as the decompression stage when it comes to the formation of tabletting defects. Nonetheless, these observations could indicate a possible strategy to reduce the incidence of tablet failure in (multi-)layered tablets as the residual radial stress has shown to be one of the strongest predictors for the occurrence of tabletting defects [9].

Although creating tablets with precise layers may be difficult in practice, they do not have to be arranged perfectly as long as the softer material is placed more towards the perimeter of the tablet.

7. Conclusions

An automated workflow, requiring minimal user input, has been developed to extract density-dependent elastic and Drucker-Prager Cap (dDPC) parameters from experimental data. Powder mixtures with micro-crystalline cellulose (MCC, plastic) and dibasic calcium phosphate dihydrate (DCPD, brittle) were used as a model system. Finite

Table 1
The maximum and residual stresses for the tablets with segregated layers of MCC and DCPD with spatial configurations as shown in Fig. 13. All stress values are in MPa. Various dimensionless stress ratios are also given. Configurations with the softer material (MCC) near the perimeter of the tablet show lower residual radial stresses as well as lower ratios of residual radial to axial stress.

Layer arrangement:	Horizontal		Vertical		Staircase	
Material at die wall:	MCC	DCPD	MCC	DCPD	MCC	DCPD
σ_z^{max}, Maximum axial stress	532	532	509	496	521	519
σ_r^{max}, Maximum radial stress	359	359	334	292	346	347
σ_r^{res}, Residual radial stress	71	71	64	82	55	67
$\sigma_r^{max}/\sigma_z^{max}$	0.67	0.67	0.64	0.59	0.66	0.67
$\sigma_r^{res}/\sigma_z^{max}$	0.13	0.13	0.13	0.17	0.11	0.13

element method (FEM) simulations using the parametrisation workflow reliably reproduced the experimental compaction curves of all materials, giving an expected error of 2.5% of the maximum compaction pressure. The observed chipping of some tablets was suggested to result from a concentration of shear stresses at the bottom edge of the tablet. Moreover, we report a novel mixing methodology that predicts the compaction behaviour of a binary mixture by using the isostress assumption. Parameters for binary mixtures were generated using only experimental data of the isolated constituent powders. FEM simulations using these generated parameters accurately predicted the compaction curves of the binary mixtures, giving an expected error of 4.8% of the maximum compaction pressure. Furthermore, the mixing methodology resulted in qualitatively similar stress profiles for the tablet when compared to the parametrisation workflow using experimental data. We thereby conclude that the workflow and mixing methodology are two key developments towards the digital design of novel powder formulations.

Investigating the dependence of mixing model predictions on the homogeneity of the powder mixture revealed that placing the softer material closer to the die wall lowers the residual radial stress. This trend may potentially be used to reduce the residual radial stress in layered tablets and thereby also the frequency of tabletting defects. Compaction curves of horizontally layered powder beds were found to strongly resemble the homogeneous mixture, giving an expected deviation of 4.5% of the maximum compaction pressure. This resemblance suggests that the stress is isotropically distributed between the materials, supporting the isostress assumption, and that the mixing methodology is insensitive to small changes in the homogeneity of the powder mixture. Subsequently, this also implies the existence of a representative volume element for binary powder mixtures, justifying the continuum representation of pharmaceutical powders. An open question is how well the assumptions of the mixing model hold when the particle size difference between components becomes large. In such cases, it might become necessary to define mixing rules depending on the relative number of particle contacts and total surface-area fraction instead of just the volume fraction. The development of such mixing rules may be further complicated by highly irregular particle shapes of which the surface area is hard to predict. Nonetheless, the accuracy of the current mixing model shows promise that the simulation of more intricate powder formulations might be possible as well.

Declaration of Competing Interest

The authors declare that they have no known competing financial interests or personal relationships that could have appeared to influence the work reported in this paper.

Acknowledgements

This project has been financed by Novo Nordisk A/S (Bagsværd, Denmark). The authors would also like to thank Karolina Wszola for providing assistance with the tablet crushing experimentation.

Appendix A. Supplementary data

Supplementary data to this article can be found online at https://doi.org/10.1016/j.powtec.2022.117381. Additional material to this publication can also be found on Apollo, the institutional repository of the University of Cambridge, at https://www.repository.cam.ac.uk/handle/1810/336083.

References

[1] A.S. Rana, S.L.H. Kumar, Manufacturing defects of tablets, Review 3 (6) (2013) 200–206, https://doi.org/10.22270/jddt.v3i6722.
[2] A. Baroutaji, K. Bryan, M. Sajjia, S. Lenihan, Mechanics and Computational Modeling of Pharmaceutical Tabletting Process, in: Reference Module in Materials Science and Materials Engineering, Elsevier, Walthm, MA, USA, 2017 https://doi.org/10.1016/B978-0-12-803581-8.09269-9.
[3] S.G. Begum, A.S. Bai, G. Kalpana, P. Mounika, J.A. Chandini, Review on tablet manufacturing machines and tablet manufacturing defects, Indian Res. J. Pharm. Sci. 5 (2) (2018) 1479–1490.
[4] A.K. Nayak, J. Malakar, K.K. Sen, Gastroretentive drug delivery technologies: current approaches and future potential, J. Pharmaceut. Edu. Res. 1 (2) (2010) 1.
[5] U.K. Mandal, B. Chatterjee, F.G. Senjoti, Gastro-retentive drug delivery systems and their in vivo success: a recent update, Asian J. Pharm. Sci. 11 (5) (2016) 575–584, https://doi.org/10.1016/j.ajps.2016.04.007.
[6] H.P. Shah, S.T. Prajapati, C. Patel, Gastroretentive drug delivery systems: from conception to commercial success, J. Critic. Rev. 4 (2) (2017) 10.
[7] J. Freiesleben, The opportunity costs of poor quality, Quality Assurance J. 9 (1) (2005) 3–10, https://doi.org/10.1002/qaj.309.
[8] S.L. Kweder, S. Dill, Drug shortages: the cycle of quantity and quality, Clin. Pharmacol. Ther. 93 (3) (2013) 245–251, https://doi.org/10.1038/clpt.2012.235.
[9] S. Paul, Y. Baranwal, Y.-C. Tseng, An insight into predictive parameters of tablet capping by machine learning and multivariate tools, Int. J. Pharm. 599 (2021) 120439, https://doi.org/10.1016/j.ijpharm.2021120439.
[10] A. Michrafy, D. Ringenbacher, P. Tchoreloff, Modelling the compaction behaviour of powders: application to pharmaceutical powders, Powder Technol. 127 (3) (2002) 257–266.
[11] I. Sinka, J. Cunningham, A. Zavaliangos, The effect of wall friction in the compaction of pharmaceutical tablets with curved faces: a validation study of the drucker-prager cap model, Powder Technol. 133 (1-3) (2003) 33–43.
[12] L. Han, J. Elliott, A. Bentham, A. Mills, G. Amidon, B. Hancock, A modified drucker-prager cap model for die compaction simulation of pharmaceutical powders, Int. J. Solids Struct. 45 (10) (2008) 3088–3106.
[13] V.S. Deshpande, N.A. Fleck, Isotropic constitutive models for metallic foams, J. Mech. Phys. Solids 48 (6) (2000) 1253–1283, https://doi.org/10.1016/S0022-5096(99)00082-4.
[14] V.S. Deshpande, N.A. Fleck, Multi-axial yield behaviour of polymer foams, Acta Mater. 49 (10) (2001) 1859–1866, https://doi.org/10.1016/S1359-6454(01)00058 1.
[15] A.L. Gurson, Continuum theory of ductile rupture by void nucleation and growth: part i-yield criteria and flow rules for porous ductile media, J. Eng. Mater. Technol. 99 (1) (1977) 2–15, https://doi.org/10.1115/1 3443401.
[16] H. Diarra, V. Mazel, V. Busignies, P. Tchoreloff, Comparative study between drucker-prager/cap and modified cam-clay models for the numerical simulation of die compaction of pharmaceutical powders, Powder Technol. 320 (2017) 530–539, https://doi.org/10.1016/j.powtec.2017.07 077.
[17] C.-Y. Wu, B. Hancock, A. Mills, A. Bentham, S. Best, J. Elliott, Numerical and experimental investigation of capping mechanisms during pharmaceutical tablet compaction, Powder Technol. 181 (2) (2008) 121–129.
[18] L.H. Han, J. Elliott, S. Best, R. Cameron, A. Bentham, A. Mills, G. Amidon, B. Hancock, Numerical simulation on pharmaceutical powder compaction, Materials Science Forum, Vol. 575, Trans Tech Publ 2008, pp. 560–565.
[19] M.S. Kadiri, A. Michrafy, The effect of punch's shape on die compaction of pharmaceutical powders, Powder Technol. 239 (2013) 467–477, https://doi.org/10.1016/j.powtec.2013.02.022.
[20] A. Krok, M. Peciar, R. Fekete, Numerical investigation into the influence of the punch shape on the mechanical behavior of pharmaceutical powders during compaction, Particuology 16 (2014) 116–131, https://doi.org/10.1016/j.partic.2013.12.003.
[21] L.H. Han, P.R. Laity, R.E. Cameron, J.A. Elliott, Density and plastic strain evaluations using small-angle X-ray scattering and finite element simulations for powder compacts of complex shape, J. Mater. Sci. 46 (18) (2011) 5977–5990, https://doi.org/10.1007/s10853-011-5559-8.
[22] C. Shang, I.C. Sinka, J. Pan, Constitutive model calibration for powder compaction using instrumented die testing, Exp. Mech. 52 (7) (2011) 903–916, https://doi.org/10.1007/s11340-011-9542-8.
[23] R. Furukawa, Y. Chen, A. Horiguchi, K. Takagaki, J. Nishi, A. Konishi, Y. Shirakawa, M. Sugimoto, S. Narisawa, Numerical evaluation of the capping tendency of microcrystalline cellulose tablets during a diametrical compression test, Int. J. Pharm. 493 (1) (2015) 182–191, https://doi.org/10.1016/j.ijpharm.2015.07.029.
[24] V. Busignies, B. Leclerc, P. Porion, P. Evesque, G. Couarraze, P. Tchoreloff, Investigation and modelling approach of the mechanical properties of compacts made with binary mixtures of pharmaceutical excipients, Eur. J. Pharm. Biopharm. 64 (1) (2006) 51–65, https://doi.org/10.1016/j.ejpb.2006.03.010.
[25] V. Busignies, P. Evesque, P. Porion, B. Leclerc, P. Tchoreloff, Mechanical properties of compacts made with binary mixtures of pharmaceutical excipients of three different kinds, AIP Conf. Proc. 1145 (1) (2009) 240–243, https://doi.org/10.1063/1.3179902.
[26] G. Bano, Z. Wang, P. Facco, F. Bezzo, M. Barolo, M. Ierapetritou, A novel and systematic approach to identify the design space of pharmaceutical processes, Comput. Chem. Eng. 115 (2018) 309–322, https://doi.org/10.1016/j.compchemeng.2018.04.021.
[27] H.M. Zawbaa, S. Schiano, L. Perez-Gandarillas, C. Grosan, A. Michrafy, C.-Y. Wu, Computational intelligence modelling of pharmaceutical tabletting processes using bio-inspired optimization algorithms, Adv. Powder Technol. 29 (12) (2018) 2966–2977, https://doi.org/10.1016/j.apt.2018.11.008.
[28] S. Dai, B. Xu, Z. Zhang, J. Yu, F. Wang, X. Shi, Y. Qiao, A compression behavior classification system of pharmaceutical powders for accelerating direct compression tablet formulation design, Int. J. Pharm. 572 (2019) 118742, https://doi.org/10.1016/j.ijpharm.2019.118742.
[29] A.L.P. Queiroz, W. Faisal, K. Devine, H. Garvie-Cook, S. Vucen, A.M. Crean, The application of percolation threshold theory to predict compaction behaviour of

pharmaceutical powder blends, Powder Technol. 354 (2019) 188–198, https://doi.org/10.1016/j.powtec.2019.05.027.
[30] C.-Y. Wu, S.M. Best, A.C. Bentham, B.C. Hancock, W. Bonfield, A simple predictive model for the tensile strength of binary tablets, Eur. J. Pharm. Sci. 25 (2) (2005) 331–336, https://doi.org/10.1016/j.ejps.2005.03.004.
[31] C.-Y. Wu, S.M. Best, A.C. Bentham, B.C. Hancock, W. Bonfield, Predicting the tensile strength of compacted multi-component mixtures of pharmaceutical powders, Pharm. Res. 23 (8) (2006) 1898–1905, https://doi.org/10.1007/s11095-006-9005-6.
[32] G.K. Reynolds, J.I. Campbell, R.J. Roberts, A compressibility based model for predicting the tensile strength of directly compressed pharmaceutical powder mixtures, Int. J. Pharm. 531 (1) (2017) 215–224, https://doi.org/10.1016/j.ijpharm.2017.08.075.
[33] C. Sun, A novel method for deriving true density of pharmaceutical solids including hydrates and water-containing powders, J. Pharm. Sci. 93 (3) (2003) 646–653, https://doi.org/10.1002/jps.10595.
[34] M. Kuentz, H. Leuenberger, Pressure susceptibility of polymer tablets as a critical property: a modified heckel equation, J. Pharm. Sci. 88 (2) (1999) 174–179, https://doi.org/10.1021/js980369a.
[35] J.N. Goodier, S.P. Timoshenko, Theory of Elasticity, McGraw-Hill Companies, Inc. New York, 1951.
[36] J.T. Fell, J.M. Newton, Determination of tablet strength by the diametral-compression test, J. Pharm. Sci. 59 (5) (1970) 688–691, https://doi.org/10.1002/jps.2600590523.
[37] E. Ryshkewitch, Compression strength of porous sintered Alumina and Zirconia, J. Am. Ceram. Soc. 36 (2) (1953) 65–68, https://doi.org/10.1111/j.1151-2916.1953.tb12837.x.
[38] R.M. Nedderman, Statics and Kinematics of Granular Materials, Cambridge University Press, Cambridge, 2005.
[39] T. Sinha, R. Bharadwaj, J.S. Curtis, B.C. Hancock, C. Wassgren, Finite element analysis of pharmaceutical tablet compaction using a density dependent material plasticity model, Powder Technol. 202 (1) (2010) 46–54, https://doi.org/10.1016/j.powtec.2010.04.001.
[40] C.-Y. Wu, O. Ruddy, A. Bentham, B. Hancock, S. Best, J. Elliott, Modelling the mechanical behaviour of pharmaceutical powders during compaction, Powder Technol. 152 (1-3) (2005) 107–117.
[41] S. Garner, J. Strong, A. Zavaliangos, The extrapolation of the Drucker-Prager/Cap material parameters to low and high relative densities, Powder Technol. 283 (2015) 210–226, https://doi.org/10.1016/j.powtec.2015.05.027.
[42] K. Hibbitt, B. Karlsson, P. Sorensen, Abaqus: User's manual: Hibbitt, Hibbitt, Karlsson & Sorensen, Pennsylvania, 1988.
[43] H.E. Krex, Maskin ståbi, Teknisk forlag, København, 1978.
[44] H. Diarra, V. Mazel, V. Busignies, P. Tchoreloff, FEM simulation of the die compaction of pharmaceutical products: influence of visco-elastic phenomena and comparison with experiments, Int. J. Pharm. 453 (2) (2013) 389–394, https://doi.org/10.1016/j.ijpharm.2013.05.038.
[45] T. Sinha, J.S. Curtis, B.C. Hancock, C. Wassgren, A study on the sensitivity of drucker-rager cap model parameters during the decompression phase of powder compaction simulations, Powder Technol. 198 (3) (2010) 315–324, https://doi.org/10.1016/j.powtec.2009.10.025.
[46] H. Diarra, V. Mazel, A. Boillon, L. Rehault, V. Busignies, S. Bureau, P. Tchoreloff, Finite Element Method (FEM) modeling of the powder compaction of cosmetic products: comparison between simulated and experimental results, Powder Technol. 224 (2012) 233–240, https://doi.org/10.1016/j.powtec.2012.02.058.
[47] S. Ohsaki, K. Kushida, Y. Matsuda, H. Nakamura, S. Watano, Numerical study for tableting process in consideration of compression speed, Int. J. Pharm. 575 (2020) 118936, https://doi.org/10.1016/j.ijpharm.2019.118936.
[48] V. Mazel, V. Busignies, H. Diarra, P. Tchoreloff, Measurements of elastic moduli of pharmaceutical compacts: a new methodology using double compaction on a compaction simulator, J. Pharm. Sci. 101 (6) (2012) 2220–2228, https://doi.org/10.1002/jps.23122.
[49] S. Abdul, S.S. Poddar, A flexible technology for modified release of drugs: multi layered tablets, J. Controlled Release 97 (3) (2004) 393–405, https://doi.org/10.1016/j.jconrel.2004.03.034.
[50] S.R. Vaithiyalingam, V.A. Sayeed, Critical factors in manufacturing multi-layer tablets-ssessing material attributes, in-process controls, manufacturing process and product performance, Int, J. Pharm. 398 (1) (2010) 9–13, https://doi.org/10.1016/j.ijpharm.2010.07.025.
[51] C.-Y. Wu, J.P.K. Seville, A comparative study of compaction properties of binary and bilayer tablets, Powder Technol. 189 (2) (2009) 285–294, https://doi.org/10.1016/j.powtec.2008.04.026.